Nonlocal Effects in Flows of Wormlike Micellar Solutions

Chloé Masselon,* Jean-Baptiste Salmon, and Annie Colin†

LOF, unité mixte CNRS–Rhodia–Bordeaux 1, 178 avenue du Docteur Schweitzer, F-33608 Pessac Cedex, France

(Received 19 July 2007; published 25 January 2008)

The flow curve of wormlike micelles usually exhibits a stress plateau $\sigma^\star$ separating high and low viscosity branches, leading to shear-banded flows. We study the flow of semidilute wormlike micellar systems in a confined geometry: a straight microchannel. We characterize their local rheology thanks to particle image velocimetry. We show that flow curves cannot be described by a simple constitutive equation linking the local shear stress to the local shear rate. We demonstrate the existence of nonlocal effects in the flow of wormlike micellar systems and make use of a theoretical framework allowing the measurement of correlation lengths.

DOI: 10.1103/PhysRevLett.100.038301 PACS numbers: 83.80.Qr, 83.60.Fg, 83.85.Ei

Wormlike micelles are long, cylindrical aggregates of self-assembled surfactants that dynamically break and recombine [1]. Those systems exhibit a characteristical flow curve shear stress vs shear rate $\sigma = f(\dot{\gamma})$ with a stress plateau $\sigma^\star$, separating two branches of low and high viscosity, and corresponding to different structures [2]. On the stress plateau, and at applied rates of shear, macroscopic bands of different $\dot{\gamma}$ and micellar orientations coexist [3–6]. As in an equilibrium transition, the proportion of the bands varies as $\dot{\gamma}$ is changed in the plateau. An important feature of this transition is the existence and the robustness of the $\sigma^\star$ value for a given system. In the past decades, theoretical approaches tried to account for these observations. Spenley *et al.* [7] used a reptation-reaction model, initially developed for linear rheology, and proposed a constitutive law. They found a multivalued flow curve exhibiting two stable branches separated by an unstable zone where σ decreases as a function of $\dot{\gamma}$. The main difficulty on those early models was to find out a mechanism to ensure the selection of the shear stress $\sigma^\star$ at which the high shear band appears. Various criteria such as minimization of an effective nonequilibrium free energy under flow [8], boundary conditions on the normal stress in pipe flow [9], or local maximum of the flow curve were used, but shown to be only in qualitative agreement with experimental data. Then a major improvement in the theoretical description was achieved by taking into account stress propagation across the interface [10–15]. This stress flux may arise either from the Brownian diffusion of polymer to-and-fro across the interface, or from van der Waals, Coulomb, or hydrodynamic interactions between polymer chains through the interface. It has been demonstrated that the introduction of this diffusion term in the constitutive law ensures a robust $\sigma^\star$ selection [14,15]. At this stage, experimental evidence of these nonlocal terms is still missing; i.e., the breakdown of the relation linking the shear rate to the shear stress has never been reported before. To probe these mechanisms in even more details, we choose to study the rheology of wormlike micelles in a confined geometry: a straight microchannel. Contrary to Couette and cone-and-plate cells or even large pipes [16–18], such a confined planar Poiseuille flow dramatically enhances the effect of nonlocal terms. The main originality of our work is to demonstrate the existence of nonlocal effects in the flow of a wormlike micellar system on two well-known systems and to propose a theoretical framework allowing the measurement of correlation lengths.

Our study mainly focuses on cetylpyridinium chloride (CP^+, Cl^-) and sodium salycilate (Na^+, Sal^-) in a 0.5 M NaCl brine at 22 °C [19], at 6 wt % with a molar ratio $[Sal]/[CPCl] = 0.5$. We then expand our observations and analysis to another wormlike micellar system: a 0.3 M solution of cetyltrimethylammonium bromide (CTAB) in a 0.405 M sodium nitrate brine (Na^+, NO_3^-) at 25 °C [20]. Both systems range in the semidilute regime far from the isotropic-nematic transition in concentration.

We study the flow of wormlike micellar systems in a homemade straight ''canyon'' microchannel [21] of a large aspect ratio (height 1 mm and width $w \approx 200$ μm). The pressure-driven flow is imposed thanks to a pressure controller with pressure drops $\Delta P = 50$–2000 mbar. The canyon geometry is well approximed by two infinite parallel planes: stream lines follow the direction X of the channel; velocity profiles are Poiseuille-like in the transverse direction Z (canyon width) and almost uniform along the canyon height. Velocity profiles in this confined geometry are measured using particle image velocimetry [22]. In this purpose the fluid is seeded with small particles (Invitrogen FluoSpheres 1 μm; volumic fraction 4×10^{-5}%). Images in the X-Z plane of the channel width w are acquired using an inverted fluorescent microscope, at a 40× magnification, at middle height of the channel (depth of field ≈ 1 μm), and far enough from the inlet of the channel to measure fully developed profiles. A CCD camera coupled to an intensifier (Hamamatsu and R&D Vision) allows us to record couples of images and thus to access local velocities up to ≈ 1 m/s with a spatial resolution $\Delta Z \approx 1$ μm in the plane of the flow.

Figure 1 shows velocity profiles for the CPCl-Sal 6 wt % at different ΔP, plotted against the normalized coordinate

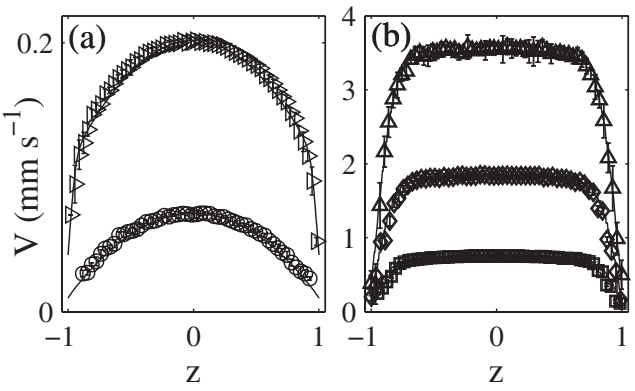

FIG. 1. Velocity profiles at (a) (○) $\Delta P = 200$, (▷) 300, (b) (□) 400, (◇) 500, and (△) 600 mbar; solid lines correspond to the modelized profiles according to Eq. (2) with the same fitting parameters for all of them and a standard deviation std = 83 μm s^{-1} (CPCl-Sal).

$z = 2Z/w$. Below 200 mbar, velocity profiles correspond to Poiseuille-like flows. At 300 mbar, thin highly sheared bands start to nucleate at the lateral walls. For higher ΔP, the width z_v of these bands increases, and the profiles correspond to plug flows, with lower viscosity bands near the walls. Widths z_v are easily determined from the neat change in the slope of the profiles. At every imposed pressure drop, significant slippage is observed at the walls. Slip velocities V_{slip} are experimentally determined by linear fits of the last points of the profiles near the walls. We observe that $V_{\text{slip}} \sim A(\Delta P/L)^{\alpha}$ with $A = 6.4 \times 10^{-11}$ S.I. and $\alpha = 3.2$, yet their contributions to the maximal velocity V_{max} remain almost constant ($V_{\text{slip}} \approx 0.15 V_{\text{max}}$). Visible nonpolarized light experiments were also performed in the same canyon geometry [see Fig. 2(a)]. For the lower ΔP (<300 mbar), homogeneous intensities throughout the width of the channel are observed. Above 300 mbar, darker bands start to nucleate at the walls, and their widths z_d increase with ΔP. These refraction index changes are probably due to variations of the texture of the wormlike micelles. Furthermore Fig. 2(c) shows the spatiotemporal evolution of these bands below $\Delta P = 700$ mbar. At those ΔP they are stable in space and time, yet they display significant fluctuations above. Figure 3 depicts the width z_v of the highly sheared bands inferred from the profiles displayed in Fig. 1, as a function of the measured widths z_d of the bands observed using visible light. It shows those darker bands correspond to the highly sheared bands nucleating at the walls above 300 mbar.

From the velocity profiles in such a microchannel flow, we can deduce the local rheological behavior [23–25]. Indeed, starting from the Stokes equation, assuming our geometry is well approximated by two infinite parallel planes, in the stationary regime and in the lubrication approximation, for any fluid the local shear stress σ is given by

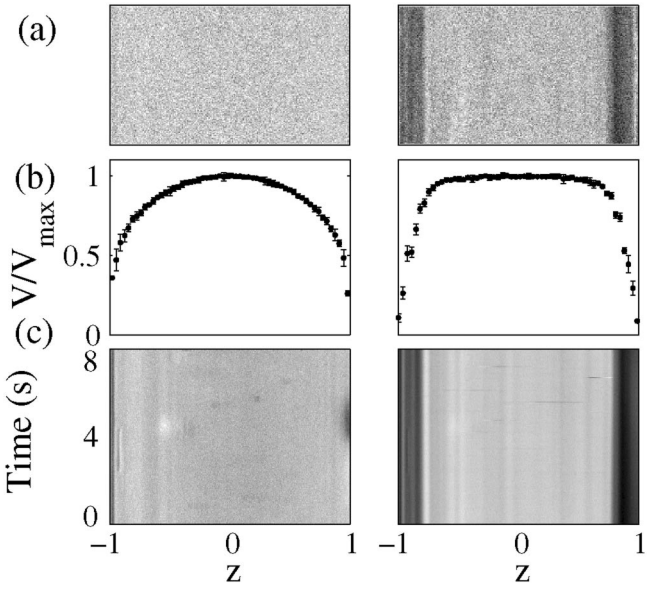

FIG. 2. (a) Visible light experiments, and (b) corresponding normalized velocity profiles at $\Delta P = 300$ (left) and 500 mbar (right). (c) Space-time plots of the same data. For those visible light data, an homogeneous reference at $\Delta P = 200$ mbar is substracted (CPCl-Sal).

$$\sigma(Z) = \frac{\partial P}{\partial X} Z = \frac{\Delta P}{L} \frac{w}{2} z, \tag{1}$$

L being the length of the channel, and $\partial P/\partial X$ the local pressure gradient. To derive the previous relation, we assume that $\partial P/\partial X$ is given by $\Delta P/L$, since entrance and exit effects are not significant. Indeed, rough estimates of the entrance and exit lengths for shear thinning fluids [26] lead to distances smaller than 70 μm in our experiments, i.e., to distances at least a hundred times smaller than the length of the channel. Besides, as the local shear rate $\dot{\gamma}$ is simply given by the local slope in the velocity profile, each Z position in the channel corresponds to a pair $(\sigma, \dot{\gamma})$. Hence from a single profile, we can access the whole flow curve. The *local* flow curves obtained by such a procedure are depicted in Fig. 4, as the *global* one determined by the shear-rate-imposed mode of a rheometer (TA Instruments ARG2) using a sanded cone-and-plate

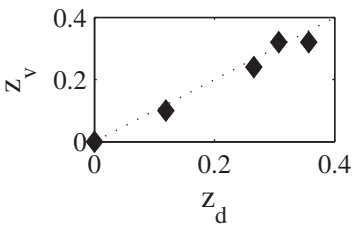

FIG. 3. Width of the highly sheared band z_v vs width of the dark band observed in visible light z_d. The widths have been normalized by $w/2$, where w is the width of the channel. The dotted line corresponds to $z_v = z_d$ (CPCl-Sal).

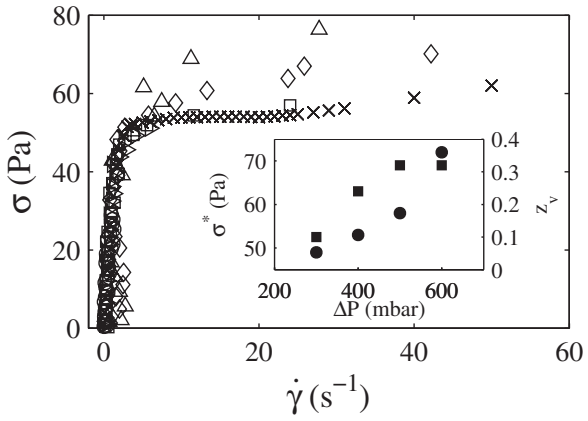

FIG. 4. Flow curve from a rheometer using a cone-and-plate cell (×), flow curve deduced from the velocity profiles at 200 (○), 300 (▷), 400 (□), 500 (◇), and 600 mbar (△). Inset: (●) stress plateau $\sigma^\star$ vs pressure drop ΔP; (■) width of the highly sheared band z_v vs ΔP (CPCl-Sal).

cell. There is quite good agreement between these local and global rheological behaviors, but only for $\dot{\gamma} < 10\ \mathrm{s}^{-1}$, corresponding to the highly viscous branch. Above, significant discrepancies are observed. The rheological behavior of the highly sheared branch seems to vary as a function of the applied ΔP. We focus on the values of the stress $\sigma^\star$ at the interface between the two bands deduced from z_v using Eq. (1). The inset of Fig. 4 shows clearly that $\sigma^\star$ increases significantly with the applied ΔP. In other words, z_v vs ΔP does not grow as much as it should if $\sigma^\star$ was constant. Note that local velocimetry experiments performed in a Couette cell (without strong shear stress gradient) or in large pipes (which is not a confined geometry) evidenced a constant $\sigma^\star$ with an increasing applied $\dot{\gamma}$ on the same system [5,16–18]. However, our experiments in a confined geometry reveal that a simple description $\sigma = f(\dot{\gamma})$ with a unique value of $\sigma^\star$ is not sufficient to describe the flow for the whole studied range of ΔP. This point is highly striking and shows that stress in wormlike micellar systems depends on other variables than $\dot{\gamma}$. We show thereafter that nonlocal descriptions are required to understand those phenomena. A careful theoretical analysis of the shear rate and shear stress profiles at the interface between two shear bands led Dhont [14] to the same conclusions. In order to cope with both the strong inhomogeneity of $\dot{\gamma}$ and the abnormal polymer stress across the interface, he introduced nonlocal terms in the constitutive law to model stress diffusion. From a microscopic point of view these terms may arise from propagation of short or long range interactions between wormlike micellar chains across the interface. At steady state this leads to

$$\sigma(Z) = \eta[\dot{\gamma}(Z)]\dot{\gamma}(Z) - D\frac{\partial^2\dot{\gamma}(Z)}{\partial Z^2}. \qquad (2)$$

The first term $R(\dot{\gamma}) = \eta[\dot{\gamma}(Z)]\dot{\gamma}(Z)$ is the contribution to σ due to a flow in an infinite geometry with no effect of the boundary conditions, in the absence of shear banding. The term $D\partial^2\dot{\gamma}/\partial Z^2$ is the nonlocal term. It expresses the smoothing of interfaces between bands. In planar shear flow, this model allows a robust selection of the stress plateau value $\sigma^\star$ [14,15]. In order to compare our data with this constitutive equation, we need to model $R(\dot{\gamma})$ and solve Eq. (2) in a planar Poiseuille flow. We assume $R(\dot{\gamma})$ is a multivalued function presenting two separated branches. For $\dot{\gamma} < \dot{\gamma}_1$, the low sheared branch is Newtonian, $R(\dot{\gamma}) = \eta\dot{\gamma}$; for $\dot{\gamma} > \dot{\gamma}_1$, the high sheared branch is shear thinning $R(\dot{\gamma}) = A\dot{\gamma}^n$. To solve Eq. (2), two boundary conditions are required. First, the flow is axisymmetric which leads to $\dot{\gamma}(0) = 0$. Second, $\dot{\gamma}$ at the wall and the slip velocities are experimentally determined from the velocity profiles. Remembering Eq. (1), we solve Eq. (2) and fit the free parameters. Figure 1 displays a comparison between this model and our experimental data. A single set of parameters ($D = 2.1 \times 10^{-10}$ Pa s m^2, $\dot{\gamma}_1 = 5\ \mathrm{s}^{-1}$, $\eta = 30$ Pa s, $A = 17$ S.I., and $n = 0.5$) allows us to perfectly fit all the profiles with a standard deviation of 83 μm s^{-1} [27]. Correlation lengths involved in the nonlocal process can be deduced by $l = [D/\eta(\dot{\gamma})]^{1/2}$. In the plateau region l ranges from 3 to 22 μm, in agreement with recent indirect measurements [28]. Clearly, these high characteristic lengths cannot be related to the mesh size. However, we believe that they are physically meaningful and are related to the structure induced by local concentration fluctuations in the highly sheared band. We recall that visible light microscopy reveals that the high shear band appears to be black, suggesting the existence of concentration fluctuations at a length scale larger than the micrometer (see Fig. 2). Note also, that l remains small in comparison to the gap of classical rheometers (0.5–1 mm) which induces that

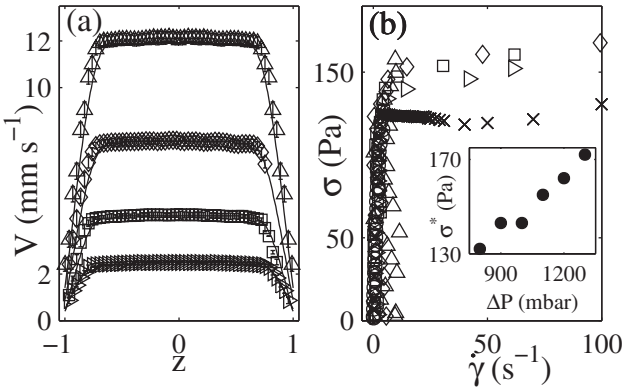

FIG. 5. (a) Velocity profiles at (▷) $\Delta P = 1000$, (□) 1100, (◇) 1200, and (△) 1300 mbar; solid lines correspond to the modelized profiles according to Eq. (2) with the same fitting parameters for all of them and a standard deviation std = 398 μm s^{-1}. $V_{\mathrm{slip}} \sim A(\Delta P/L)^\alpha$ with $A = 3.510^{-22}$ S.I. and $\alpha = 5.7$. (b) Corresponding local flow curves, and global flow curve measured with a rheometer (×). Inset: stress plateau vs pressure drop (CTAB-$NaNO_3$).

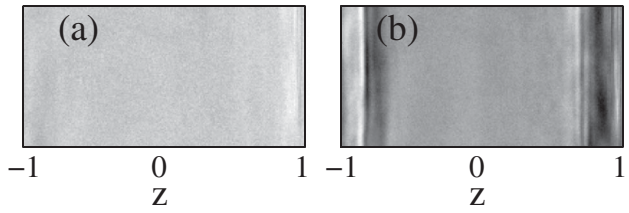

FIG. 6. Visible light experiments at $\Delta P =$ (a) 700 and (b) 1300 mbar. A homogeneous reference at $\Delta P = 200$ mbar is subtracted (CTAB-$NaNO_3$).

nonlocal effects cannot be sounded in these geometries, even by performing local measurements. Figure 5 sums up the main results we obtained on a similar wormlike micellar system: CTAB-$NaNO_3$. Figure 5(a) depicts velocity profiles at different pressure drops. At low ΔP the same results were obtained by Degré *et al.* [29]. Figure 5(b) shows the global and local flow curves. The inset shows the evolution of $\sigma^\star$ with ΔP. The solid lines on Fig. 5(a) correspond to the fits with Eq. (2) with a single set of parameters ($D = 2.01 \times 10^{-10}$ Pa s m^2, $\dot{\gamma}_1 = 4$ s^{-1}, $\eta =$ 30 Pa s, $A = 39$ S.I., and $n = 0.391$). Correlation lengths l in the plateau region range between 3 and 8 μm and are much larger than the ones measured by Radulescu *et al.* [30] using kinetic experiments. Note that these discrepancies might be due to the difficulty to properly separate in the kinetics the different steps involved in the displacement of the interface (instability, reconstruction, and front propagation) [31]. Visible light experiments (Fig. 6) also exhibit strong refractive index fluctuations in the highly sheared bands, which appear to be stable in space and time under a critical ΔP of 1500 mbar. Note that in this case, the highly sheared bands exhibit both darker and brighter area, the interface is therefore blurred, which differs from the CPCl-Sal system. That phenomenon seems more complex, yet might be due to the smaller range of accessible correlation lengths.

To conclude, we evidenced a generic behavior of wormlike micellar solutions in the semidilute regime. Nonlocal terms are required to describe the stress propagation across the interface in shear-banded flow. These nonlocal terms have a huge importance in the selection of the position of the interface in planar Poiseuille flow. We point out that correlation lengths involved in this process are very large, yet correspond to the length scale involved in the concentration fluctuations. Recent studies [31,32] suggest the existence of instabilities captured by Fielding *et al.* [33] using a modified Johnson Segalman model. To investigate such instabilities further, experiments at higher ΔP are planned, as well as quantitative comparisons with microscopic models [34].

We thank Région Aquitaine for fundings and A. Ajdari, G. Degré, P. Nghe, M. Joanicot, and P. Tabeling for fruitful discussions.

*chloe.masselon-exterieur@eu.rhodia.com
†annie.colin-exterieur@eu.rhodia.com

[1] M. E. Cates, Macromolecules **20**, 2289 (1987).
[2] I. Wunderlich *et al.*, Rheol. Acta **26**, 532 (1987).
[3] M. M. Britton *et al.* Phys. Rev. Lett. **78**, 4930 (1997).
[4] S. Lerouge *et al.*, Phys. Rev. Lett. **81**, 5457 (1998).
[5] J.-B. Salmon *et al.*, Phys. Rev. Lett. **90**, 228303 (2003).
[6] L. Bécu *et al.*, Phys. Rev. Lett. **93**, 018301 (2004).
[7] N. A. Spenley *et al.*, Phys. Rev. Lett. **71**, 939 (1993).
[8] G. Porte *et al.*, J. Phys. II (France) **7**, 459 (1997).
[9] T. C. B. McLeish, J. Polym. Sci., Part B: Polym. Phys. **25**, 2253 (1987).
[10] J. Krug *et al.*, J. Stat. Phys. **44**, 535 (1986).
[11] J. R. A. Pearson, J. Rheol. (N.Y.) **38**, 309 (1994).
[12] P. D. Olmsted *et al.*, Phys. Rev. A **41**, 4578 (1990).
[13] P. D. Olmsted *et al.*, Phys. Rev. E **56**, R55 (1997).
[14] J. K. G. Dhont, Phys. Rev. E **60**, 4534 (1999).
[15] C. Y. D. Lu *et al.*, Phys. Rev. Lett. **84**, 642 (2000).
[16] R. W. Mair *et al.*, J. Rheol. (N.Y.) **41**, 901 (1997).
[17] A. F. Mendez-Sanchez *et al.*, J. Rheol. (N.Y.) **47**, 1455 (2003).
[18] M. M. Britton *et al.*, Eur. Phys. J. B **7**, 237 (1999).
[19] J.-F. Berret *et al.*, Phys. Rev. E **55**, 1668 (1997).
[20] E. Cappelaere *et al.*, Colloid Polym. Sci. **276**, 1050 (1998).
[21] P. Guillot *et al.*, Langmuir **22**, 6438 (2006).
[22] J. G. Santiago *et al.*, Exp. Fluids **25**, 316 (1998).
[23] H. Mullermohnssen *et al.*, J. Rheol. (N.Y.) **34**, 223 (1990).
[24] B. M. Marin-Santibanez *et al.*, Langmuir **22**, 4015 (2006).
[25] G. Degré *et al.*, Appl. Phys. Lett. **89**, 024104 (2006).
[26] M. Collins *et al.*, AIChE J. **9**, 98 (1963).
[27] We compute the standard deviation of the difference between all the experimental profiles and the theoretical ones, standard deviation of vector X being std $= \sqrt{\frac{1}{N-1}\sum_{i=1}^{N}(X_i - \overline{X})^2}$, where $\overline{X}$ is the mean value of X, and N is its length. The range of fitting parameters we use here corresponds to a deviation std$/V_{\max}$ between fits and data of less than 4%.
[28] P. Ballesta *et al.*, J. Rheol. (N.Y.) **51**, 1047 (2007).
[29] G. Degré, Ph.D. thesis, Université Paris 6, 2007.
[30] O. Radulescu *et al.*, Europhys. Lett. **62**, 230 (2003).
[31] S. Lerouge *et al.*, Phys. Rev. Lett. **96**, 088301 (2006); S. Lerouge (private communication).
[32] R. Ganapathy *et al.*, Phys. Rev. Lett. **96**, 108301 (2006).
[33] S. M. Fielding *et al.*, Phys. Rev. Lett. **96**, 104502 (2006).
[34] L. F. Rossi *et al.*, J. Non-Newtonian Fluid Mech. **136**, 79 (2006).